

Temperature Effect and Fermi Surface Investigation in the Scanning Tunneling Microscopy of $\text{Bi}_2\text{Sr}_2\text{CaCu}_2\text{O}_8$

K.-K. Voo¹, W. C. Wu², H.-Y. Chen³, and C.-Y. Mou^{1,4}

¹*Department of Physics, National Tsing-Hua University, Hsinchu 300, Taiwan*

²*Department of Physics, National Taiwan Normal University, Taipei 11650, Taiwan*

³*Texas Center for Superconductivity and Department of Physics, University of Houston, Houston, TX 77204, USA*

⁴*Physics Division, National Center for Theoretical Sciences, P.O. Box 2-131, Hsinchu 300, Taiwan*
(November 21, 2018)

Based on a Fermi liquid picture, the temperature effect on the impurity-induced spatial modulation of local density of states (LDOS) is investigated for the d -wave superconductor $\text{Bi}_2\text{Sr}_2\text{CaCu}_2\text{O}_8$, in the context of scanning tunneling microscopy (STM). It is found that stripe-like structure exists even in the normal state due to a local-nesting mechanism, which is different from the octet scattering mechanism proposed by McElroy *et al.* [Nature **422**, 592 (2003)] in the d -wave superconducting (d SC) state. The normal-state spectra, when Fourier-transformed into the reciprocal space, can reveal the information of the entire Fermi surface at a single measuring bias, in contrast to the point-wise tracing proposed by McElroy *et al.* This may serve as another way to check the reality of Landau quasiparticles in the normal state. We have also re-visited the spectra in the d SC state and pointed out that, due to the Umklapp symmetry of the lattice, there should exist additional peaks in the reciprocal space, but experimentally yet to be found.

PACS numbers: 74.70.Pq, 74.20.Rp, 74.25.Ld

I. INTRODUCTION

A fundamental question on the high- T_c cuprates remains after more than fifteen years of the discovery of the material. It is still not clear whether the cuprates are systems of Fermi liquid (FL), non-FL with exotic orders such as the stripes [1], or systems with more intricate co-existence of different states of matter [2]. In fact, this question arises in both their superconducting and normal states. Besides, it is not unusual that different experimental probes give different implications – the experimental findings are not yet converged.

A substantial progress in the STM measurement has made it another route to this problem. Not only STM looks directly into the real space, but also it can be readily connected to the reciprocal space, so-called the Fourier transformed STM (FT-STM). Data of the low (and fixed) temperature STM on $\text{Bi}_2\text{Sr}_2\text{CaCu}_2\text{O}_8$ (BSCCO) was claimed to be an excellent manifestation of the FL behavior [3,4]. But, since the cuprates are such involved systems, one should be more careful to nail down the conclusion. Whether the observed STM modulation [5] is solely the Friedel stripe arising from the quasiparticle (QP) interference, or the Zaanen-Kivelson stripe [1] coexisting with the Friedel stripe, is actually an issue still in debate (see the contradictory data of Refs. [6] and [7]) [8]. Even if the stripes can be attributed to the QP interference alone, it is still crucial to ask how well do the quasiparticles behave? How is the extension of the “Fermi-arc”, and up to what temperatures they survive [9]? So far there has been few finite-temperature and normal-state STM studies on the cuprates [10]. These are the major concerns of the present paper.

Based on the FL scenario, an abstract model named

the “octet” scattering model [5] has successfully ascribed the experimentally observed FT-STM peaks of the LDOS modulation to the quantum interference of the QPs. Later concrete single-impurity scattering calculations [11,3,4] also supported that. The occurrence of FT-STM peaks and their evolution with the bias change give information of the Fermi surface (FS) of the measured system which are consistent with previous results from the angle-resolved photoemission spectroscopy. This provides a strong identification of a Friedel stripe out of the Zaanen-Kivelson stripe. But nevertheless, some weak non-dispersive peaks, which could be due to a coexisting Zaanen-Kivelson stripe, may also exist [6–8].

It is important to investigate how far the FL picture can be pushed, especially when the temperature is raised and the system enters the normal state. We thus have performed similar FL-based calculations at different temperatures to study the Friedel stripes, for the reference of future experiments in checking the validity of the FL picture. It is found that stripe-like structure exists even in the normal state. This may be counterintuitive to the octet model, since the octets should vanish in the normal state. We argue that apart from the octets, a local-nesting property of the FS (especially important in the normal state) can also give rise to sizable joint-DOS, and hence sizable QP scattering.

In Sec. II, we formulate the problem as the scattering from a single impurity. In Sec. III, we present the calculated spectra at different temperatures and the essential features are remarked. In Sec. IV, the physical origin of the normal-state spectra are elucidated. It is noted that in the normal state, the information of the entire FS can be revealed from the data of a single measuring bias. This is in contrast to the point-wise tracing out in the d SC state. Sec. V is a closing section. In Appendix,

we make a comment to the present FT-STM data, pointing out that some additional peaks should exist in the measurement.

II. FORMALISM

Since the single-impurity scattering model was proved to be an excellent start for understanding the STM features in the d SC state, we proceed to study the finite-temperature phenomena based on it. We will be interested in those regions away from the impurity neighborhood. We consider the following Hamiltonian

$$H = H_0 + H_I, \quad (1)$$

where H_0 is the usual BCS mean-field Hamiltonian

$$H_0 = \sum_{\mathbf{k}, \sigma} \xi_{\mathbf{k}} c_{\mathbf{k}\sigma}^\dagger c_{\mathbf{k}\sigma} + \sum_{\mathbf{k}} \left[\Delta_{\mathbf{k}} c_{\mathbf{k}\uparrow}^\dagger c_{-\mathbf{k}\downarrow}^\dagger + \text{H.c.} \right] \quad (2)$$

with $\xi_{\mathbf{k}}$ and $\Delta_{\mathbf{k}}$ the band dispersion relative to chemical potential and the superconducting gap function respectively, and H_I is the part associated with an impurity at site $\mathbf{0}$,

$$H_I = \sum_{\langle i,j \rangle, \sigma} \delta t_{ij} c_{i\sigma}^\dagger c_{j\sigma} + \sum_{\langle i,j \rangle} \left[\delta \Delta_{ij} c_{i\uparrow}^\dagger c_{j\downarrow}^\dagger + \text{H.c.} \right] + V_0 \left(c_{0\uparrow}^\dagger c_{0\uparrow} + c_{0\downarrow}^\dagger c_{0\downarrow} \right). \quad (3)$$

Parameter δt is the deviation of local hopping, $\delta \Delta$ is the deviation of local pairing potential, and V_0 is the on-site impurity potential. This is a simplified model but nevertheless should be enough to bring out the essential features of interest.

It is convenient to apply the Nambu representation for the reciprocal and real-space operators:

$$\hat{C}_{\mathbf{k}} \equiv \begin{bmatrix} c_{\mathbf{k}\uparrow} \\ c_{-\mathbf{k}\downarrow}^\dagger \end{bmatrix} \quad \text{and} \quad \hat{C}_j \equiv \begin{bmatrix} c_{j\uparrow} \\ c_{j\downarrow}^\dagger \end{bmatrix}, \quad (4)$$

which are related to each other via the Fourier transformation

$$\hat{C}_{\mathbf{k}} = \frac{1}{\sqrt{N}} \sum_j e^{-i\mathbf{k}\cdot\mathbf{r}_j} \hat{C}_j. \quad (5)$$

Here the sum is over all the lattice sites \mathbf{r}_j . Define a 2×2 energy matrix

$$\hat{\epsilon}_{\mathbf{k}} \equiv \begin{bmatrix} \xi_{\mathbf{k}} & \Delta_{\mathbf{k}} \\ \Delta_{\mathbf{k}}^* & -\xi_{\mathbf{k}} \end{bmatrix}, \quad (6)$$

thus

$$H_0 = \sum_{\mathbf{k}} \hat{C}_{\mathbf{k}}^\dagger \hat{\epsilon}_{\mathbf{k}} \hat{C}_{\mathbf{k}}. \quad (7)$$

Similarly

$$H_I \equiv \sum_{i,j} \hat{C}_i^\dagger \hat{u}_{ij} \hat{C}_j + \text{H.c.}, \quad (8)$$

where the matrix elements \hat{u}_{ij} are to be given later.

Since we are interested in the real-space STM spectra which measure the LDOS, we need to know the real-space, equal-site, single-particle Green's functions. Define a single-particle Green's function matrix

$$\hat{G}(\mathbf{r}_i, \mathbf{r}_j, \tau) = -\langle T_\tau \hat{C}_i(\tau) \hat{C}_j^\dagger(0) \rangle, \quad (9)$$

the LDOS is then given by

$$D(\mathbf{r}, \omega) = -\frac{1}{2\pi} \text{Im} [G_{11}(\mathbf{r}, \mathbf{r}, i\omega_n \rightarrow \omega + i0^+) - G_{22}(\mathbf{r}, \mathbf{r}, -i\omega_n \rightarrow -\omega - i0^+)], \quad (10)$$

where $G_{\alpha\beta}$ is an element of the 2×2 Green's function matrix in (9), being Fourier-transformed to the Matsubara-frequency space

$$\hat{G}(\mathbf{r}_i, \mathbf{r}_j, i\omega_n) = \int_0^\beta d\tau e^{i\omega_n \tau} \hat{G}(\mathbf{r}_i, \mathbf{r}_j, \tau). \quad (11)$$

Following the standard technique, the full \hat{G} in (9) can be expanded in terms of H_I given by (8),

$$\begin{aligned} \hat{G}(\mathbf{r}_i, \mathbf{r}_j, \tau) &= \hat{G}^0(\mathbf{r}_i, \mathbf{r}_j, \tau) \\ &+ \int_0^\beta d\tau_1 \langle T_\tau \hat{C}_i(\tau) \sum_{k,\ell} \hat{C}_k^\dagger(\tau_1) \hat{u}_{k\ell} \hat{C}_\ell(\tau_1) \hat{C}_j^\dagger(0) \rangle \\ &+ O(\hat{u}^2), \end{aligned} \quad (12)$$

where, $\hat{G}^0(\mathbf{r}_i, \mathbf{r}_j, \tau) \equiv \hat{G}^0(\mathbf{r}_i - \mathbf{r}_j, \tau)$ is the mean-field “non-interacting” \hat{G} when $H_I = 0$.

The terms included in H_I in (3) are given explicitly here. For BSCCO, we consider a square lattice of lattice constant a . In the case of a single, extended and weak impurity, we consider local deviations δt_1 and $\delta \Delta_1$ which couple the impurity site and its nearest neighbors, and δt_2 and $\delta \Delta_2$ which couple the impurity's nearest neighbors and its next nearest neighbors. Consequently, there are 17 non-vanishing \hat{u} matrices in (8):

$$\begin{aligned} \hat{u}_{0,0} &= \begin{bmatrix} V_0 & 0 \\ 0 & -V_0 \end{bmatrix}, \quad \hat{u}_{0,\pm a\hat{x}} = \begin{bmatrix} \delta t_1 & \delta \Delta_1 \\ -\delta \Delta_1 & -\delta t_1 \end{bmatrix}, \\ \hat{u}_{0,\pm a\hat{y}} &= \begin{bmatrix} \delta t_1 & -\delta \Delta_1 \\ \delta \Delta_1 & -\delta t_1 \end{bmatrix}, \\ \hat{u}_{a\hat{x},2a\hat{x}} &= \hat{u}_{-a\hat{x},-2a\hat{x}} = \hat{u}_{a\hat{y},2a\hat{y}} = \hat{u}_{-a\hat{y},-2a\hat{y}} \\ &= \begin{bmatrix} \delta t_2 & \delta \Delta_2 \\ -\delta \Delta_2 & -\delta t_2 \end{bmatrix}, \\ \hat{u}_{a\hat{x},a\hat{x}\pm a\hat{y}} &= \hat{u}_{-a\hat{x},-a\hat{x}\pm a\hat{y}} = \hat{u}_{a\hat{y},a\hat{y}\pm a\hat{x}} = \hat{u}_{-a\hat{y},-a\hat{y}\pm a\hat{x}} \\ &= \begin{bmatrix} \delta t_2 & -\delta \Delta_2 \\ \delta \Delta_2 & -\delta t_2 \end{bmatrix}. \end{aligned} \quad (13)$$

Hamiltonians similar to this have been successfully used by Tang and Flatté [11] to explain the resonant STM

spectra for Ni doped BSCCO, and by Wang and Lee [3] and Zhang and Ting [4] to explain the energy-dependent modulation of the FT-STM spectra on superconducting BSCCO. Since we consider the weak impurity scattering limit, \hat{G} in (12) is only calculated up to the first order of \hat{u} (the Born limit). The first order term has already included the essential interference effect of the QPs. A strong impurity is expected to give new features (such as a bound state) only at the immediate neighborhood of the impurity. Eq. (12) is then reduced to

$$\hat{G}(\mathbf{r}_i, \mathbf{r}_j, i\omega_n) = \hat{G}^0(\mathbf{r}_i - \mathbf{r}_j, i\omega_n) + \sum_{k, \ell} \hat{G}^0(\mathbf{r}_i - \mathbf{r}_k, i\omega_n) \hat{u}_{k\ell} \hat{G}^0(\mathbf{r}_\ell - \mathbf{r}_j, i\omega_n). \quad (14)$$

The first term on the right is translationally invariant. Spatial variation of the LDOS at a fixed energy comes only from the second term. It is related to the STM spectrum discussed in Ref. [5] via $\mathbf{r}_i = \mathbf{r}_j = \mathbf{r}$ and $i\omega_n \rightarrow eV + i0^+$, where $e = |e|$ is the electron charge and V is the bias voltage. Its Fourier transform is the FT-STM spectrum. We will be discussing the second term on the right throughout this paper.

Note that the thermal Fermi distribution function never appears in the full Green's function \hat{G} here. It arises only when the Matsubara-frequency sum is involved, i.e., when the impurity is dynamic and inelastic scattering occurs. Since we have assumed an elastic impurity, our Green's function depends on temperature only through the gap magnitude $\Delta(T)$ which should change with temperature.

In our calculation, we have used a 800×800 square lattice with the impurity at the center. We have chosen a simple but reasonable impurity potential, $2\delta t_1 = 4\delta t_2 = -2\delta\Delta_1 = -4\delta\Delta_2 = V_0$ and have assumed that these scales are small and in the perturbative limit. For $\xi_{\mathbf{k}}$, we use a tight-binding band, $\xi_{\mathbf{k}} = t_1(\cos k_x + \cos k_y)/2 + t_2 \cos k_x \cos k_y + t_3(\cos 2k_x + \cos 2k_y)/2 + t_4(\cos 2k_x \cos k_y + \cos k_x \cos 2k_y)/2 + t_5 \cos 2k_x \cos 2k_y - \mu$ (lattice constant $a \equiv 1$), with $t_{1-5} = -0.60, 0.16, -0.05, -0.11, 0.05$ eV and chemical potential $\mu = -0.12$ eV, appropriate for an optimally-doped BSCCO [12]. In addition, the superconducting gap is taken to be $\Delta_{\mathbf{k}} = \Delta(T)(\cos k_x - \cos k_y)/2$ with $\Delta(T)$ the temperature-dependent gap magnitude. Besides, we have introduced a finite broadening $\gamma = 2$ meV to the Green's function, such that $eV + i0^+$ is replaced by $eV + i\gamma$.

III. STM AND FT-STM SPECTRA

In Fig. 1, we present the temperature evolution of the real-space STM spectra at two different negative bias voltages. The case of positive bias voltage will not be discussed as they are qualitatively the same. The gap magnitudes are taken from $\Delta(T=0) = 44$ to $\Delta(T_c) = 0$ meV to simulate the transition from the superconducting

to the normal state. At a distance of several lattice constants away from the impurity, oscillating Friedel stripes are seen in all panels, even in the case of normal states [$\Delta(T) = 0$]. Spectra with a similar ratio of $e|V|/\Delta(T)$ share a similar behavior, such as those in Fig. 1(b), (c) with $e|V|/\Delta(T) = 25/44, 15/26 \sim 0.57$. On the other hand, spectra at zero $\Delta(T)$ is robust at the change of V [see Fig. 1(g) and (h)]. Comparing the relative intensities of the modulations, we see that the strongest modulations (at a fixed bias voltage) appear at temperatures near T_c . One more important feature to note is that the different ripples live in well-separated patches of space. The ripples do not have large-area overlaps.

The Fourier-transforms of the above spectra are given in Fig. 2. Roughly speaking, there are two regimes for the spectra in the $\Delta(T) \neq 0$ superconducting state, as classified by the ratio $e|V|/\Delta(T)$. When $e|V|/\Delta(T) < 1$, there are local peaky structures that have their locations describable by the octet model [see Figs. 2(a)–(c)], in agreement with previous studies [3,4]. Previous studies discussed the cases with different eV and a fixed $\Delta(T) \approx \Delta(0)$, while in our case $\Delta(T)$ is varied (by changing the temperature). In comparison of Fig. 2(b) and (c) that have a similar ratio $e|V|/\Delta(T) \sim 0.57$, one again sees that the essential features of the spectra depend mainly on the ratio $e|V|/\Delta(T)$, as noted before in the discussion of the real-space spectra. In Fig. 3, a closer look of the locations of the interference peaks in Figs. 2(a)–(c) is given. When $e|V|/\Delta(T) > 1$ [see Figs. 2(d)–(f)], some extra peaky structures beyond the description of the octet model appear near $\mathbf{q} = 0$. These new structures are not expected to be observable in real BSCCO compound because they are related to the maximum gap part of the STM spectra (see discussion in Sec. IV), which in turn are highly inhomogeneous in space. As $\Delta(T)$ is further decreased, the strong peak at $\mathbf{q} = 0$ is suppressed and vanishes at entering the normal state.

In the normal state, the FT-STM spectra are reduced to some neat ridges instead of peaks [see Figs. 2(g) and (h)], and they are rather robust against the change of bias. They should be readily observable in practice.

As the interference peaks in the d SC states (in the regime of $e|V|/\Delta(T) < 1$) were well documented in the literature [3,4], we will only give a supplementary comment on it in Appendix. In Sec. IV we pay special attention to the normal-state spectra.

IV. ORIGIN OF THE NORMAL-STATE SPECTRA

In this section, we show that the normal-state FT-STM spectra have an intimate relationship with the underlying FS.

The pronounced feature of the FT-STM in the d SC state is that the peaks have locations depending on the bias. As long as the ratio $e|V|/\Delta(T)$ is small enough

to stay away from the maximum gap region, locations of the peaks are more or less as described by the octet model [3] – a model that assumes the dominant QP scattering comes between regions of high DOS on the FS (the octets). These are regions with the smallest velocity, which appear at the tips of the banana-shape constant energy contour ($|\xi_{\mathbf{k}}|^2 + |\Delta_{\mathbf{k}}(T)|^2 = \text{constant}$). The agreement of the low-temperature experimental observation with the picture was claimed to be good [5]. Later specific single-impurity scattering calculations [3,4] (similar to the one done in Sec. II) also supported this picture. In the normal state, such large DOS octets no longer exist. However, we point out that there exists a different mechanism which can also cause a substantial *joint*-DOS, and leads to distinguished structures in the \mathbf{q} space.

The upper panel of Fig. 4 shows a typical normal-state FT-STM spectrum in an extended Brillouin zone (BZ). The underlying FS is also shown in the lower panel. Comparing the two panels, it is readily seen that the “ridges” in the spectrum are of the same shape as the FS, but having twice the size, and differently oriented branches overlap together. The occurrence of the ridges can be understood from the scattering wave vectors drawn in the lower panel. Those wave vectors, which are pivoted at $\mathbf{q} = (m\pi/a, n\pi/a)$, $n, m \in \text{integer}$, are special in the sense that they joint *locally parallel* segments of the FS, i.e., they possess a weak “local-nesting” [13] (such nesting is the weakest possible type of nesting, or it is “marginal”). As a result, stripes in the real-space are still understood as due to the scattering on the FS.

In the normal state, there is no small and well-separated large DOS regions, therefore the stripes in real-space are smoothly deformed unlike those in the *d*SC state. An implication from the above understanding to the *d*SC state is, the new structures at higher $eV/\Delta(T)$ in Fig.2 (which were not seen by the experiment) come actually from the maximum gap regions. In either state, quasiparticles come from different directions \mathbf{v}_F to hit the impurity, get bounced back, and get interfered with some transition wave vector \mathbf{q} . Since \mathbf{v}_F and \mathbf{q} are not simply related, the orientations of the interference ripples in the patches of space are also not simply related to their orientations from the impurity. It is also obvious that within the same patch of space there will be no two crossing ripples. Therefore, to explain the “checkerboard” pattern (overlapping ripples) seen in the experiments using this picture, one needs to consider the existence of a *dilute* concentration of impurities in the system [14,15].

V. CONCLUDING REMARKS

Our perturbative approach should not be a concern regarding the validity of our discussion. In this paper, it is not our purpose to investigate the local bound states at the vicinity of the impurity. We are interested only in those regions remote from the impurity, where the in-

terference between scattered quasiparticles is expected to be the dominant process. The approach has included the interference effect lucidly.

In the literature, it was proposed that temperature could be a detrimental factor to the quasiparticles [9]. If this is true, the normal-state stripe described in this paper is expected to vanish. Stripes of a different origin may exist [1], but they are likely to differ in many aspects, such as the orientation or temperature dependence of the stripes. In our case, the real-space normal-state stripes [14] and the corresponding ridges in the FT-STM spectra reflect the information of the entire Fermi surface. If there are destructions of quasiparticle states at some Fermi surface segments, the corresponding segments of the ridges in the FT-STM spectrum should also be destroyed. The presence of a *pseudogap* in the normal state should also be signified as some missing segments of the ridges. Our study interpolates the *d*SC and normal-state STM, using an approach supported by the experiment in the *d*SC state. The “fingerprints” of the Fermi liquid under the STM probe, in the course of the superconducting-to-normal transition, are enumerated for future experiments.

ACKNOWLEDGMENTS

This work is supported by the National Science Council of Taiwan under the Grant Nos. 92-2112-M-003-009 (WCW) and 92-2811-M-007-027 (KKV and CYM). HYC thanks the support of National Center for Theoretical Sciences (Physics Division) of Taiwan during his visit.

APPENDIX: UMKLAPP SYMMETRY

In this Appendix, a brief comment is given to the experimental data in Ref. [5]. If one considers the octet model in the *d*SC state more carefully, it will be interesting to note the existence of additional peaks, which are not yet realized in current experimental data.

In Fig. 5, for a certain bias voltage, we have illustratively shown a few direct and Umklapp scattering wavevectors in the octet model [16]. In addition to the scattering vectors within the first Brillouin zone (direct), there are also vectors connecting octets in different Brillouin zones (Umklapp). When all these vectors are taken into account, there should exist FT-STM peaks as shown in the lower panel of the figure. Take an example, a new peak at the vector q'_5 is seen along the q_y axis (when the bias voltage exceeds some value). Peak at q_5 was reported by Ref. [5], but the corresponding q'_5 peak was not. The more disturbing matter is, there also exists a q'_4 peak which may come close to $q_{2,6}$ peaks (or vice versa speaking).

It may seem at odds that a mathematical Fourier transform of experimental data on a discrete lattice does not

automatically possess the Umklapp symmetry. The reason may be due to the fact that practical STM actually probes a space *more continuous* than the underlying lattice. It scans in steps *smaller* than the lattice constants, and identifies the locations of individual atoms only later, by looking at the modulation profile. The probe tip does not jump from one atom to another right on-top!

FIG. 1. Temperature dependence of the LDOS modulation surrounding the impurity. All panels are plotted within a square region, $r_x, r_y = -20 \sim 20a$, with the impurity at the center. The left and right columns show the spectra at bias $V = -15$ and -25 mV respectively, and from top to bottom the gap magnitude $\Delta(T) = 44, 26, 10,$ and 0 meV respectively. For better visualization, spectra in different panels are plotted in different intensity windows from $-x$ (deepest blue) to $+x$ (deepest red) as specified by the color scale at the bottom. The individual value of x is given at the lower-right corner of the individual panel. Those regions of the deepest blue/red have intensities below/above the window.

-
- [1] S.A. Kivelson *et al.*, cond-mat/0210683.
 - [2] S. Sachdev, Rev. Mod. Phys. **75**, 913 (2003).
 - [3] Q.-H. Wang and D.H. Lee, Phys. Rev. B **67**, 020511 (2003).
 - [4] D. Zhang and C.S. Ting, Phys. Rev. B **67**, 100506 (2003).
 - [5] K. McElroy, R.W. Simmonds, J.E. Hoffman, D.H. Lee, J. Orenstein, H. Eisaki, S. Uchida, J.C. Davis, Nature **422**, 592 (2003).
 - [6] C. Howald, H. Eisaki, N. Kaneko, M. Greven, and A. Kapitulnik, Phys. Rev. B **67**, 14533 (2003).
 - [7] J.E. Hoffman, K. McElroy, D.H. Lee, K.M. Lang, H. Eisaki, S. Uchida, J.C. Davis, Science **297**, 1148 (2002).
 - [8] We think that the possible non-dispersive FT-STM peaks reported in Ref. [7] might be due to the bilayer splitting of the electronic bands in the BSCCO compounds. The bilayer splitting [$\sim (\cos k_x - \cos k_y)^2$] is more prominent at near the antinodes, and may give rise to splitted FT-STM peaks, while some of them could be less dispersive at higher biases.
 - [9] J. Zaanen, Nature **422**, 569 (2003).
 - [10] T. Pereg-Barnea and M. Franz, cond-mat/0306712.
 - [11] J.-M. Tang and M.E. Flatté, Phys. Rev. B **66**, 060504 (2002).
 - [12] M.R. Norman, M. Randeria, H. Ding, and J.C. Campuzano, Phys. Rev. B **52**, 615 (1994).
 - [13] Such local-nesting effect is similar to the mechanism leads to the incommensurate peaks observed by the inelastic neutron scattering (INS) in LSCO or YBCO (see e.g., K.-K. Voo *et al.*, Physica C **382**, 323 (2002); cond-mat/0006312 and references therein). However, in the *d*SC state, local-nesting effect in the INS is energy dependent and gives rise to energy-dependent peak locations.
 - [14] In a real material, the real-space spectra may be seen as some crossing superpositions of stripes due to individual impurities, showing some “checkerboard” pattern. It was first pointed out by us in cond-mat/0302473 [published in Phys. Rev. B **68**, 012505 (2003)] that the existence of dilute impurities is crucial in relating this kind of calculation to the experimentally observed checkerboard pattern.
 - [15] L. Zhu, W.A. Atkinson, and P.J. Hirschfeld, cond-mat/0307228.
 - [16] For easy comparison, our notations are chosen in a way corresponding to those in Ref. [5].

FIG. 2. Temperature dependence of the FT-STM spectra (corresponding to the real-space results in Fig. 1) in the first Brillouin zone $q_x, q_y = -\pi/a \sim \pi/a$. Left and right columns are for $V = -15$ and -25 mV respectively. From top to bottom, $\Delta(T) = 44, 26, 10,$ and 0 meV respectively. The spectrum in each panel is plotted in an intensity window from x_l to x_u . The values of x_l and x_u are specified at the bottom of each panel, and the color scales are shown at the bottom of the figure.

FIG. 3. This figure shows that the positions of the interference peaks (indicated by arrows) depend mainly on the ratio $e|V|/\Delta(T)$. Spectra in Figs. 2(a)-(c) are scanned along $\mathbf{q}/a = (0.56\pi, 0.56\pi) \rightarrow (0, 0) \rightarrow (0.8\pi, 0)$. It is seen that Figs. 2(b) and (c), which have a similar $e|V|/\Delta(T)$ ratio, have similar peak positions and intensities. For easier comparison, the intensity of the spectrum in Fig. 2(a) is enlarged by a factor of 2.

FIG. 4. (Upper panel) The FT-STM spectrum of a normal-state system at a bias of -23 mV. The ridge-like structure is a typical feature of all normal-state spectra. (Lower panel) Several of the wavevectors on the above ridges are shown in the extended Brillouin zones. They are wavevectors having a local-nesting property, i.e., they joint locally parallel parts of the Fermi surface (as illustrated by pairs of red lines).

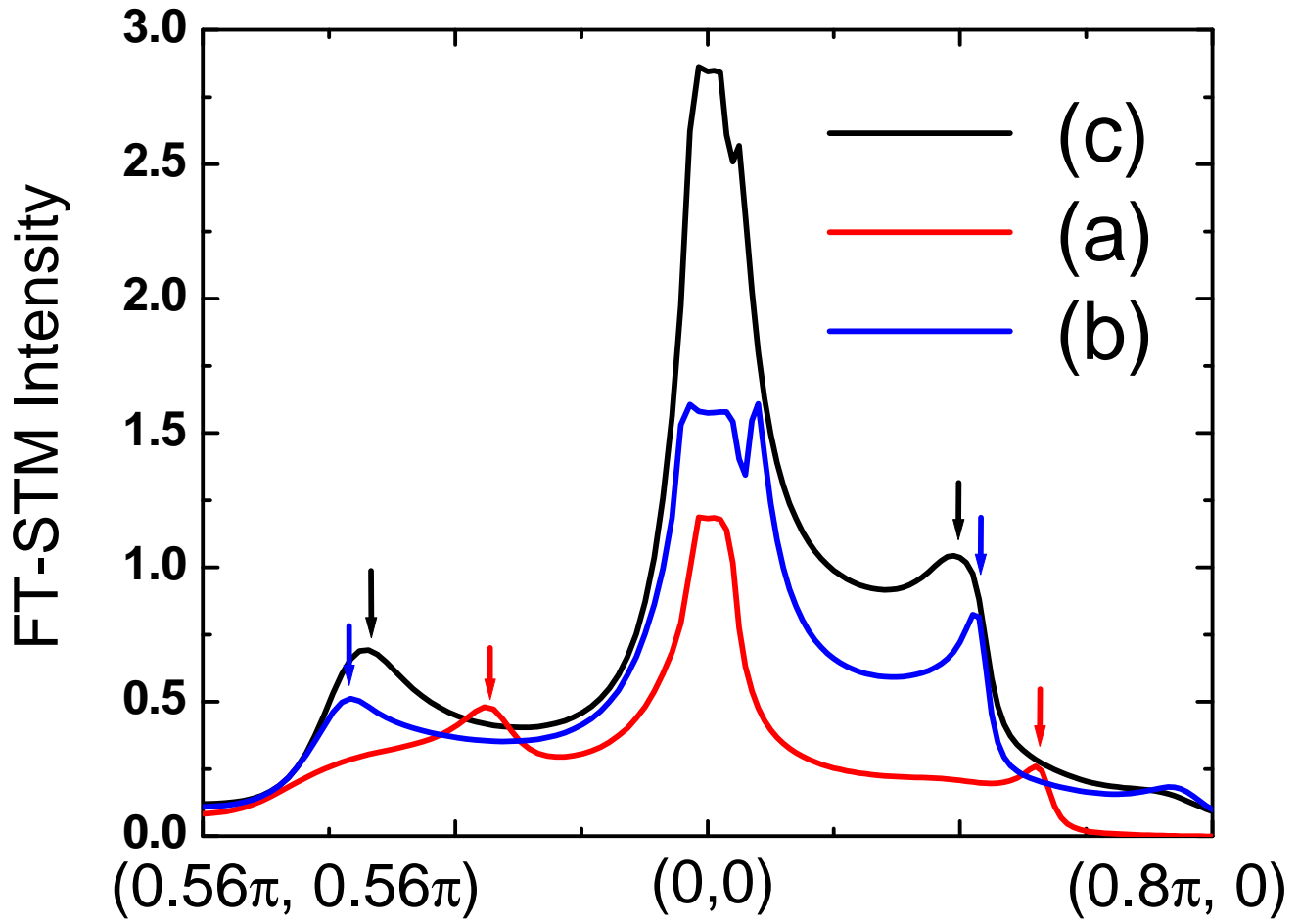
FIG. 5. (a) For illustration, a few of the scattering wavevectors in the octet model (the octets are indicated as circles) are shown. Wavevectors discussed by McElroy *et al.* [5] are shown in blue, while the Umklapp wavevectors (which were not discussed in Ref. [5]) are in red. (b) Locations of all the wavevectors connecting all the octets. The Umklapp wavevectors are in red.

This figure "fig1.jpg" is available in "jpg" format from:

<http://arxiv.org/ps/cond-mat/0308149v1>

This figure "fig2.jpg" is available in "jpg" format from:

<http://arxiv.org/ps/cond-mat/0308149v1>



This figure "fig4.jpg" is available in "jpg" format from:

<http://arxiv.org/ps/cond-mat/0308149v1>